Article

Catalytic Reduction of Acetone by [(bpy)Rh]: A Theoretical Mechanistic Investigation and Insight into Cooperativity Effects in This System

Mark A. Iron, Andreas Sundermann, and Jan M. L. Martin

J. Am. Chem. Soc., **2003**, 125 (37), 11430-11441• DOI: 10.1021/ja028489e • Publication Date (Web): 22 August 2003

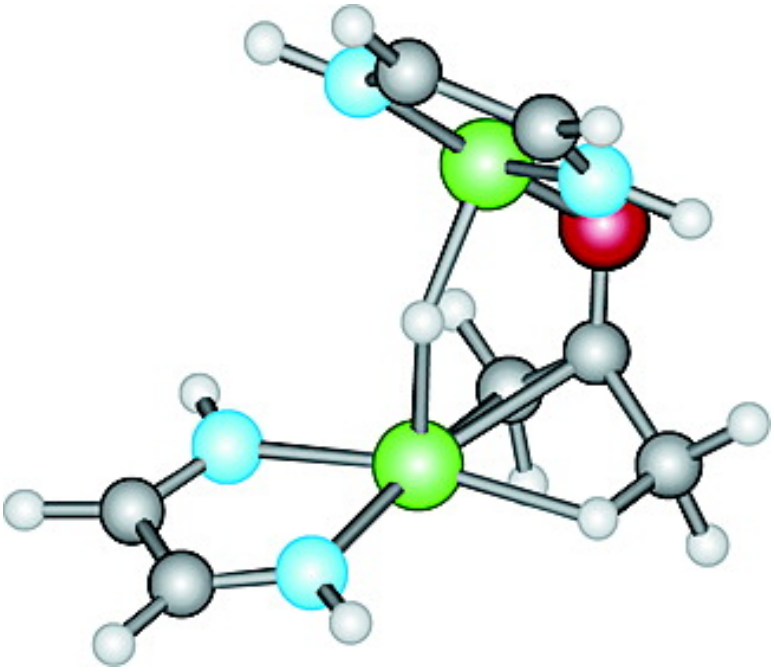

J|A|C|S
ARTICLES
Published on Web 08/22/2003

Catalytic Reduction of Acetone by [(bpy)Rh]$^+$: A Theoretical Mechanistic Investigation and Insight into Cooperativity Effects in This System

Mark A. Iron, Andreas Sundermann, and Jan M. L. Martin*

Contribution from the Department of Organic Chemistry, Weizmann Institute of Science, 76100 Rehovot, Israel

Received September 10, 2002; E-mail: comartin@wicc.weizmann.ac.il

Abstract: Lahav, Milstein, and co-workers reported that the complex [(bpy)Rh(hd)]$^+$PF$_6^-$ (bpy = substituted bipyridine ligand, hd = 1,5-hexadiene) shows catalytic activity in the hydrogenation of acetone (Töllner, K. et al. *Science* **1997**, *278*, 2100). The activity in an ordered monolayer was found to be dramatically greater than in solution. We used the DFT functional mPW1K (Lynch, B. J. et al. *J. Phys. Chem. A* **2000**, *104*, 4811) to investigate the mechanism of the homogenous reaction. The suitability of the mPW1K functional was verified by coupled cluster calculations on a model system. Bulk solvent effects were considered. Various alternative catalytic cycles were evaluated, and we found that one potential mechanism involves metal-catalyzed keto−enol tautomerization to form [(bpy)Rh(enol)]$^+$ that adds hydrogen yielding a complex with axial and equatorial hydride ligands. The reaction continues via transfer of the hydrides to the enolic C=C bond thereby forming 2-propanol and regenerating the catalyst. Another potential catalytic cycle involves formation of [(bpy)Rh(acetone)$_2$(H)$_2$]$^+$, which has a spectator solvent ligand, and initial transfer of the equatorial hydride to the carbonyl carbon of acetone. Other mechanisms involving hydrogen transfer to the acetone tautomer involved higher barriers. With an eye toward modeling multi-center catalysis, various model systems for the bpy ligand were considered. It was found that diimine (HN=CH−CH=NH) compares very well with bpy, whereas *cis*-1,2-diiminoethylene (H$_2$C=N−CH=CH−N=CH$_2$) yields a reaction profile very close to that of bpy. Finally, the system with two rhodium centers, [(diimine)Rh]$_2^{2+}$, was investigated. The results strongly suggest that an enol-type catalytic cycle occurs and that cooperativity between the two metal centers is responsible for the acceleration of the reaction in the monolayer system.

Introduction

The use of transition metal organometallic complexes as catalysts is of great importance in industry. They provide an efficient route to a variety of compounds. One major avenue of research is modifying catalysts to improve their yield and selectivity. Recently, Töllner et al.[1] reported on the solution and monolayer hydrogenation of acetone to 2-propanol by the complex (4,4′-dialkyl-2,2′-bipyridine)rhodium(hexadiene) hexafluorophosphate (alkyl = methyl or heptadecyl). The solution reactivity of similar complexes was earlier reported by Mestroni et al.,[2] and more recently by, for example, Pénicaud et al.[3] In an acetone solution (alkyl = methyl), the complex shows a low activity of 500 turnover numbers (TON) after 48 h and little selectivity between acetone and butanone. When, however, a monolayer, specifically a Langmuir−Blodgett film, is prepared from the complex (alkyl = heptadecyl), the reactivity changes dramatically, and in an aqueous acetone solution over 50 000 TON are obtained in 48 h. Moreover, the catalyst becomes selective to acetone and does not reduce butanone at all. It was hypothesised that the dramatic difference in reactivity and selectivity can be attributed to the order of the monolayer.[1]

The use of monolayers to increase catalytic reactivity has increased in recent years.[4] The order associated with such a construct can increase reactivity by reducing decomposition of the catalyst, preventing side products from forming, and/or by lowering reaction barriers. Monolayers are commonly formed, for example, as Langmuir−Blodgett films (for example, see refs 1,5−7) or assembled on the surface of a gold colloid (see, for example, refs 8,9). The reactivity of a variety of catalytic reactions has been found to be significantly enhanced by making a monolayer out of the catalyst, including alkene hydrogenation,[1,5] phenylacetylene oligomerization,[6] epoxidation,[7] ring-opening metathesis polymerization,[8] and even Sharpless asymmetric dihydroxylation.[9] In addition, the product of the monolayer catalyst can on occasion vary from the product of the solution catalyst. For example, in solution Ni(CO)$_2$(PPh$_3$)$_2$ trimerizes phenylacetylene to give 1,2,4-triphenylbenzene as the major

(1) Töllner, K.; Popovitz-Biro, R.; Lahav, M.; Milstein, D. *Science* **1997**, *278*, 2100.
(2) Mestroni, G.; Zassinovich, G.; Camus, A. *J. Organomet. Chem.* **1977**, *140*, 63.
(3) Pénicaud, V.; Maillet, C.; Janvier, P.; Pipelier, M.; Bujoli, B. *Eur. J. Org. Chem.* **1999**, *5*, 1745.
(4) Kakkar, A. *Chem. Rev.* **2002**, *102*, 3579.
(5) Petrucci, M. G. L.; Kakkar, A. *Chem. Mater.* **1999**, *11*, 269.
(6) Petrucci, M. G. L.; Kakkar, A. *Organometallics* **1998**, *17*, 1798.
(7) Benítez, I. O.; Bujoli, B.; Camus, L. J.; Lee, C. M.; Odobel, F.; Talham, D. R. *J. Am. Chem. Soc.* **2002**, *124*, 4363.
(8) Bartz, M.; Küther, J.; Seshadri, R.; Tremel, W. *Angew. Chem., Int. Ed. Engl.* **1998**, *37*, 3466.
(9) Li, H.; Luk, Y.-Y.; Mrksich, M. *Langmuir* **1999**, *15*, 4957.

10.1021/ja028489e CCC: $25.00

product (70% yield) and 1,3,5-triphenylbenzene as a trace product (<1% yield), yet when a monolayer is formed, the symmetric benzene is the major product (56%) and the asymmetric one is the minor product (23%).[6] One key element of monolayer catalysis is cooperativity between two or more metal centers. This can also be seen in solution in a bimetallic complex where each metal has a key role in the reaction. Recent examples include oxygen transfer from sulfoxides to metal-bound CO[10] and enhanced efficiency in polymerization of ethylene to form linear low-density polyethylene.[11]

Recently, Morris and co-workers reported on a combined computational and experimental investigation into the hydrogenation of ketones by Noyori-type diaminediphosphineruthenium(II) catalysts.[12,13] They found that the mechanism involves simultaneous attack on the ketone by the Ru−H and N−H bonds via a four-member transition state. Although there is some similarity to the system studied here, one key difference between the two systems, namely the lack of an N−H bond in our bpy ligand, renders the mechanism they found irrelevant here. Andersson and co-workers investigated a similar system with an amino alcohol ligand on the ruthenium(II) center.[14]

Here, we report on our computational investigation into the mechanism of the hydrogenation of acetone catalyzed by [(bpy)-Rh]$^+$. The first step in understanding the monolayer system is to understand the mechanism of the simpler solution reactivity. We used DFT methods, specifically mPW1K,[15] to investigate several possible reaction mechanisms. We have recently used this method to investigate a number of reactions of late transition metal complexes.[16,17] In addition, we determined the smallest model ligand that can be used in the calculations that adequately describes the full bpy system. This is essential for calculations on the bimetallic system as they would otherwise be beyond the limit of the computational resources available. Finally, we also provide some insight into the cooperativity effects that make the monolayer a more efficient catalytic system.

Computational Details

All calculations were carried out using Gaussian 98 Revision A.11[18] and MOLPRO 2002.3[19] running on Compaq ES40 and XP1000 workstations in our group, on Linux PC Farms belonging to the Faculty of Physics and the Faculty of Chemistry, on the SGI Origin computers of the Faculty of Chemistry and the (Israel) Inter-University Computing Center and on a mini-farm belonging to our group consisting of four Intel Pentium IV and four Intel dual Xeon 2.0 GHz PC's running Red Hat Linux 7.2.

The mPW1K (modified Perdew-Wang 1-parameter for kinetics) DFT exchange-correlation functional of Truhlar and co-workers[15] was used to investigate the reaction. This functional is based on the Perdew-Wang exchange functional[20] with Adamo and Barone's modified enhancement factor[21] and the Perdew-Wang correlation functional.[20] A larger percentage of Hatree-Fock exchange has been introduced[15] to circumvent the underestimated barrier heights typical of standard exchange-correlation functionals. It has been shown (e.g., refs 15, 16, 22, 23) that this functional generally yields much more reliable reaction barrier heights than B3LYP or other "conventional" exchange-correlation functionals.

With this functional, two basis set-RECP (relativistic effective core potential) combinations were used. The first, denoted SDD, is the combination of the Huzinaga−Dunning double-ζ basis set[24] on lighter elements with the Stuttgart−Dresden basis set-RECP combination[25] on transition metals. The second, denoted SDB-cc-pVDZ, combines the Dunning cc-pVDZ basis set[26] on the main group elements and the Stuttgart−Dresden basis set-RECP on the transition metals with an added *f*-type polarization exponent taken as the geometric average of the two *f*-exponents given in the Appendix to ref 27. Geometry optimizations were carried out using the former basis set, whereas the energetics of the reaction were calculated at these geometries with the latter basis set; this level of theory is conventionally denoted as mPW1K/SDB-cc-pVDZ//mPW1K/SDD. We have previously recommended this level of theory as better suited than the more popular B3LYP/LANL2DZ to investigate reaction mechanisms.[16]

Intrinsic reaction coordinate (IRC) calculations[28−30] were carried out at the mPW1K/SDD level on the transition states belonging to the more plausible catalytic cycles (Cycles A, B, Fa−d, G, H and J, vide infra) to confirm their connectivity.

To accurately compare the relative energetics of the two most plausible reaction cycles, single point energies of the mPW1K/SDD optimized structures of the intermediates and transition states involved in some key reaction step were calculated at the CCSD(T) level (coupled cluster ab initio method with all single and double substitutions[31] with a quasiperturbative estimate of the effect of the connected triple substitutions[32]) using the SDB-cc-pVDZ basis set.

Solvation effects were approximated using either a polarized continuum (overlapping spheres) model (PCM)[33−35] or a conductor screening model (COSMO).[36,37] In both cases, acetone ($\epsilon = 20.7$) was

(10) Fabre, S.; Findeis, B.; Trösch, D. J. M.; Gade, L. H.; Scowen, I. J.; McPartlin, M. *Chem. Commun.* **1999**, 577.
(11) Abramo, G. P.; Li, L.; Marks, T. J. *J. Am. Chem. Soc.* **2002**, *124*, 13 966.
(12) Abdur-Rashid, K.; Clapham, S. E.; Hadzovic, A.; Harvey, J. N.; Lough, A. J.; Morris, R. H. *J. Am. Chem. Soc.* **2002**, *124*, 15 104.
(13) Noyori, R.; Yamakawa, M.; Hashiguchi, S. *J. Org. Chem.* **2001**, *66*, 7931.
(14) Alonso, D. A.; Brandt, P.; Nordin, S. J. M.; Andersson, P. G. *J. Am. Chem. Soc.* **1999**, *121*, 9580.
(15) Lynch, B. J.; Fast, P. L.; Harris, M.; Truhlar, D. G. *J. Phys. Chem. A* **2000**, *104*, 4811.
(16) Iron, M. A.; Lo, H. C.; Martin, J. M. L.; Keinan, E. *J. Am. Chem. Soc.* **2002**, *124*, 7041.
(17) Iron, M. A.; Martin, J. M. L.; van der Boom, M. E. *Chem. Commun.* **2003**, 132.
(18) Frisch, M. J.; Trucks, G. W.; Schlegel, H. B.; Scuseria, G. E.; Robb, M. A.; Cheeseman, J. R.; Zakrzewski, V. G.; Montgomery, J. A., Jr.; Stratmann, R. E.; Burant, J. C.; Dapprich, S.; Millam, J. M.; Daniels, A. D.; Kudin, K. N.; Strain, M. C.; Farkas, O.; Tomasi, J.; Barone, V.; Cossi, M.; Cammi, R.; Mennucci, B.; Pomelli, C.; Adamo, C.; Clifford, S.; Ochterski, J.; Petersson, G. A.; Ayala, P. Y.; Cui, Q.; Morokuma, K.; Malick, D. K.; Rabuck, A. D.; Raghavachari, K.; Foresman, J. B.; Cioslowski, J.; Ortiz, J. V.; Stefanov, B. B.; Liu, G.; Liashenko, A.; Piskorz, P.; Komaromi, I.; Gomperts, R.; Martin, R. L.; Fox, D. J.; Keith, T.; Al-Laham, M. A.; Peng, C. Y.; Nanayakkara, A.; Gonzalez, C.; Challacombe, M.; Gill, P. M. W.; Johnson, B. G.; Chen, W.; Wong, M. W.; Andres, J. L.; Head-Gordon, M.; Replogle, E. S.; Pople, J. A. *Gaussian 98*, revision A.11; Gaussian, Inc.: Pittsburgh, PA, 2001.
(19) Amos, R. D.; Bernhardsson, A.; Berning, A.; Celani, P.; Cooper, D. L.; Deegan, M. J. O.; Dobbyn, A. J.; Eckert, F.; Hampel, C.; Hetzer, G.; Knowles, P. J.; Korona, T.; Lindh, R.; Lloyd, A. W.; McNicholas, S. J.; Manby, F. R.; Meyer, W.; Mura, M. E.; Nicklass, A.; Palmieri, P.; Pitzer, R.; Rauhut, G.; Schütz, M.; Schumann, U.; Stoll, H.; Stone, A. J.; Tarroni, R.; Thorsteinsson, T.; Werner, H.-J. MOLPRO, a package of ab initio programs designed by H.-J. Werner and P. J. Knowles, version 2002.3.
(20) Perdew, J. P.; Chevary, J. A.; Vosko, S. H.; Jackson, K. A.; Perderson, M. R.; Singh, D. J.; Fiolhais, C. *Phys. Rev. B* **1992**, *46*, 6771.
(21) Adamo, C.; Barone, V. *J. Chem. Phys.* **1998**, *108*, 664.
(22) Lynch, B. J.; Truhlar, D. G. *J. Phys. Chem. A* **2001**, *105*, 2936.
(23) Parthiban, S.; de Oliveira, G.; Martin, J. M. L. *J. Phys. Chem. A* **2001**, *105*, 895.
(24) Dunning, T. H., Jr.; Hay, P. J. In *Modern Theoretical Chemistry*; Schaefer, H. F., III, Ed.; Plenum Press: New York NY, 1977; Vol. 4.
(25) Dolg, M. In *Modern Methods and Algorithms of Quantum Chemistry*; Grotendorst, J., Ed.; John von Neumann Institute for Computing, Jülich, 2000; Vol. 1, pp 479−508.
(26) Dunning, T. H., Jr. *J. Chem. Phys.* **1989**, *90*, 1007.
(27) Martin, J. M. L.; Sundermann, A. *J. Chem. Phys.* **2001**, *114*, 3408.
(28) Fukui, K. *Acc. Chem. Res.* **1981**, *14*, 363.
(29) Gonzalez, C.; Schlegel, H. B. *J. Chem. Phys.* **1989**, *90*, 2154.
(30) Gonzalez, C.; Schlegel, H. B. *J. Phys. Chem.* **1990**, *94*, 5523.
(31) Purvis, G. D., III; Bartlett, R. J. *J. Chem. Phys.* **1982**, *76*, 1910.
(32) Raghavachari, K.; Trucks, G. W.; Pople, J. A.; Head-Gordon, M. *Chem. Phys. Lett.* **1989**, *157*, 479.
(33) Miertus, S.; Scrocco, E.; Tomasi, J. *Chem. Phys.* **1981**, *55*, 117.
(34) Miertus, S.; Tomasi, J. *Chem. Phys.* **1982**, *65*, 239.
(35) Cossi, M.; Barone, V.; Cammi, R.; Tomasi, J. *Chem. Phys. Lett.* **1996**, *255*, 327.
(36) Klamt, A.; Schüürmann, G. *J. Chem Soc., Perkin Trans. II* **1993**, 799.

used as the solvent. Strictly speaking, COSMO is more appropriate for very polar solvents, such as water, although it has been recently demonstrated that nonpolar solvents may be treated using this model.[37,38] Nevertheless, the similarity of the results obtained by both methods lends credence to their results. The static isodensity surface polarized continuum (IPCM)[39] and self-consistent isodensity PCM (SCI-PCM)[39] models were not employed because our system is positively charged, and these methods are known to behave erratically with charged systems.[37]

Results and Discussion

We performed DFT calculations on the parent 2,2′-bipyridine (bpy) system and examined a number of conceivable catalytic cycles. The 4,4′-alkyl groups are too remote to have a significant influence on the reaction. The experimental catalyst precursor used has a hexadiene ligand that was ignored as it is unlikely to have an effect on the reaction. The noncoordinating hexafluorophosphate (PF_6^-) counteranion was also ignored as it is very unlikely to enter the coordination sphere of the metal center. The hydrogenation of acetone is calculated to be exothermic by $\Delta E = -23.4$ kcal/mol or $\Delta G_{298} = -7.2$ kcal/mol.

Several different catalytic cycles were investigated. These arise from the different tautomers of acetone (ketone and enol), the two different hydride ligands (axial and equatorial) and the different initial hydride acceptors. The different catalytic cycles are as follows:

(1) Cycles A and B: initial transfer of the equatorial hydride to the carbonyl carbon of acetone;

(2) Cycle C: initial transfer of the axial hydride to the carbonyl carbon of acetone;

(3) Cycle D: initial transfer of the axial hydride to the carbonyl oxygen of acetone;

(4) Cycle E: initial transfer of the equatorial hydride to the carbonyl oxygen of acetone;

(5) Cycle F: hydrogen transfer to the enol tautomer of acetone.

Furthermore, three additional cycles were examined that include a spectator solvent molecule on the metal complex. These are as follows:

(6) Cycle G: Cycle A + solvent;

(7) Cycle H: Cycle B + solvent;

(8) Cycle I: Cycle F + solvent.

Each cycle will be discussed in full below. Finally, a catalytic cycle (Cycle J) is considered where there is cooperation between two rhodium centers.

Naming Convention. Most of the complexes discussed are derivatives of octahedra with various sites left vacant. For simplicity, the following naming convention is used. The plane of the bpy ligand is defined as equatorial, leaving two cis equatorial sites available. Perpendicular to the equatorial plane are two axial ligand sites that may or may not be occupied. Furthermore, as several catalytic cycles are examined, complexes are named according to the cycles to which they belong (uppercase letters) and their position within the cycle (numbers). For example, **A2** would be the second intermediate in Cycle A, whereas **TS(B5−6)** is the transition state connecting the fifth and sixth intermediates in Cycle B. In addition, in certain cases, the catalytic cycles may have various variants wherein the order in which ligands associate or dissociate varies. As this does not significantly change the overall catalytic cycle, they are denoted by the catalytic cycle to which they belong (capital letter) and each variant is indicated by a lower case letter. It is not uncommon that a particular intermediate belongs to more than one catalytic cycle and/or variant.

Scheme 1. Addition of Hydrogen to [(bpy)RhL]$^+$

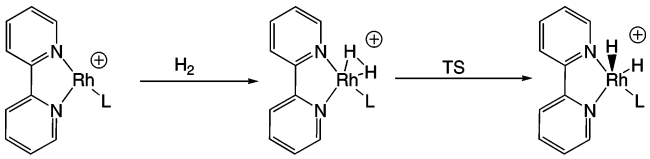

L = acetone, enol, water or nothing

Table 1. Key Interatomic Distances (Å) and Angles (°) Involved in the Addition of H_2 to [(bpy)Rh]$^+$

	[(bpy)Rh]$^+$+H_2	[(bpy)Rh(H_2)]$^+$	TS	[(bpy)RhH_2]$^+$
H−H	0.738	0.840	1.517	1.866
Rh−H_{ax}	∞	1.725	1.524	1.499
Rh−H_{eq}	∞	1.725	1.548	1.551
H_{eq}−Rh−H_{ax}		28.2	59.2	75.4

Addition of Hydrogen. The addition of a molecule of hydrogen to the rhodium center can occur either to the bare [(bpy)Rh]$^+$ complex or to the solvated [(bpy)RhL]$^+$ (L = acetone, enol or H_2O) complexes. Regardless, the reaction follows the same pathway outlined in Scheme 1. In the first step, a nonclassical η^2-H_2 dihydrogen complex is formed. This complex is transformed to a complex with an equatorial hydride (herein H_{eq}) and an axial hydride (herein H_{ax}). The formation of the σ-H_2 complex can be described as the transfer of electron density from the metal center to the σ^* orbital of the dihydrogen ligand and from the filled σ-orbital of H_2 to a vacant metal d-orbital, much like the Dewar−Chatt−Duncanson model for the coordination of ethylene.[40−42] The oxidative addition can thus be viewed as a complete transfer of electrons forming the dihydride complex. As a result, the calculated barriers, as expected, are on the order of a few kcal/mol, often barely more than the reaction energy.

Table 1 lists the key interatomic distances and angles in the complexes without a spectator ligand. The results with a spectator ligand are similar. The transition state has an imaginary frequency of 145i cm^{-1} corresponding to H−H bond activation and movement of H_{ax} and H_{eq} to their respective positions. In the dihydride complex, H_{ax} is bent from the idealized axial position (H−Rh−H = 90°) toward H_{eq}. Table 2 lists the reaction barriers and energies for each of the cycles calculated. In a number of cases, the barrier for H−H activation is too small to be precisely determined at the level of theory employed. This will be discussed in further detail when discussing another similarly problematic barrier, **TS(A4−5)** (vide infra).

Catalytic Cycles A and B: Initial Transfer of H_{eq} to the Carbonyl Carbon of Acetone. Cycle A involves the addition of hydrogen to acetone in its keto form. This cycle starts with [(bpy)Rh]$^+$. The order of addition of hydrogen and acetone gives

(37) Cramer, C. J. In *Essentials of Computational Chemistry: Theories and Models*; John Wiley & Sons: Chichester, UK, 2002, pp 347−383.
(38) Dolney, D. M.; Hawkins, G. D.; Winget, P.; Liotard, D. A.; Cramer, C. J.; Truhlar, D. G. *J. Comput. Chem.* **2000**, *21*, 340.
(39) Foresman, J. B.; Keith, T. A.; Wiberg, K. B.; Snoonian, J.; Frisch, M. J. *J. Phys. Chem.* **1996**, *100*, 16 098.
(40) Dewar, M. J. S. *Bull. Soc. Chim. Fr.* **1951**, *18*, C71.
(41) Chatt, J.; Duncanson, L. A. *J. Chem. Soc.* **1953**, 2939.
(42) Kubas, G. J. *J. Organomet. Chem.* **2001**, *635*, 37.

Scheme 2. Reaction Pathways for Cycles Aa, Ab, and B[a]

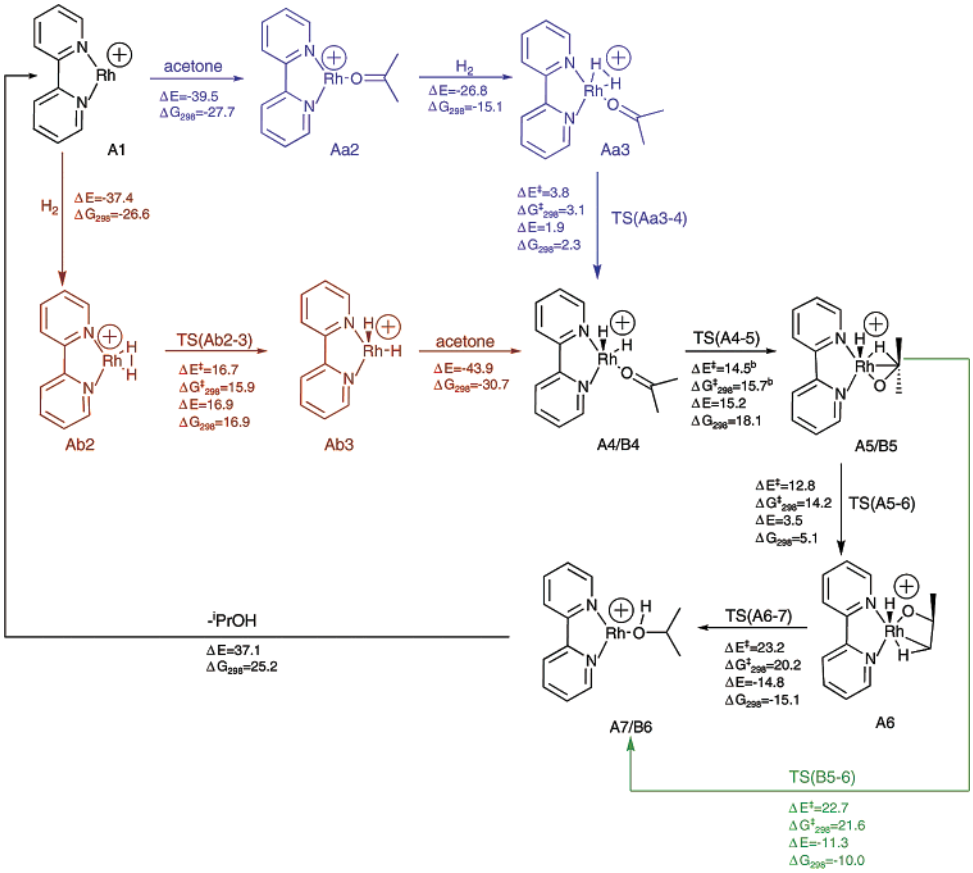

[a] Energies are reported in kcal/mol. Blue signifies Cycle Aa and red Cycle Ab, whereas black designates complexes common to both. Green denotes the step unique to Cycle B. [b]See text.

Table 2. Reaction Energies (ΔG_{298}) and Barrier Heights ($\Delta G^{\ddagger}_{298}$) for the Addition of Hydrogen to [(bpy)RhL]$^{+}$ (in kcal/mol)

L	cycle	σ-H_2	TS	$(H)_2$
bare	Ab	−26.6	15.9	16.9
ace	Aa	−15.1	3.1	2.3
^{i}PrOH	Ae	−14.5	[a]	3.1
^{i}PrOH	Af	−14.5	[a]	3.7
enol	Fa	−0.8	[a]	−2.5
	Fb	−0.8	[a]	−0.9
	Fc	−0.8	[a]	2.8
	Fd	−0.8	2.5	2.4
	Fe	−9.3	3.2	2.7
	Ff	−12.6	[a]	4.9
	Fg	−12.6	[a]	3.3
	Fh	−9.3	3.2	2.7

[a] Barrier too small to be accurately determined; see text.

rise to the two variants, Cycle Aa and Cycle Ab. In the former, the addition of acetone is first, whereas in the latter, the addition of hydrogen occurs first. These catalytic cycles are shown in Scheme 2 along with the calculated reaction energies and barrier heights of the individual steps. Figure 1 depicts the calculated structures involved in this reaction. The reaction profiles of Cycles A, B, and Fa (vide infra) are depicted in Figure 2 (similar to those in refs 43−45). The intermediates and transition states involved in the addition of hydrogen have already been discussed (vide supra). The part of interest here begins with intermediate **A4**, the acetone complex with an axial and an equatorial hydride. After the formation of **A4**, Cycles Aa and Ab follow the same pathway.

In this catalytic cycle, H_{eq} is transferred in the initial step to the carbonyl carbon of the acetone, yielding an *iso*-propoxy complex (**A5**) with an agostic interaction between the rhodium center and the newly formed C−H bond. This complex then rotates around the CO bond leading to a complex where the agostic interaction now involves one of the methyl C−H bonds (**A6**). Transfer of H_{ax} to the oxygen gives the oxygen bound 2-propanol complex (**A7**). The loss of 2-propanol regenerates the catalyst, thus starting a new catalytic cycle.

The first transition state, **TS(A4−5)**, corresponds to the transfer of H_{eq} to the carbonyl carbon. This transition state would appear to rest below the product of the reaction with $\Delta E^{\ddagger} = -0.7$ kcal/mol and $\Delta G^{\ddagger}_{298} = -2.3$ kcal/mol for the reverse reaction. Nonetheless, one must remember that using the mPW1K/SDD optimized geometry for the mPW1K/SDB-cc-pVDZ energy profile is an approximation that can lead to errors—especially in cases of small energy differences, such as the apparent reversal of transition state and product in this reaction step. In fact, on the mPW1K/SDD reaction profile, $\Delta E^{\ddagger} = 1.6$ kcal/mol for the reverse reaction. Furthermore, the correction to the energy used in order to calculate G_{298} is calculated using the rigid-rotor-harmonic-oscillator approximation. Similar problems arise in the H−H bond activation in σ-H_2 complexes (vide supra). What is significant here is the bottom line that the barrier is too small to have an impact on the reaction

(43) Widauer, C.; Grützmacher, H.; Ziegler, T. *Organometallics* **2000**, *19*, 2097.
(44) Landis, C. R.; Feldgus, S. *Angew. Chem., Int. Ed. Engl.* **2000**, *39*, 2863.
(45) Feldgus, S.; Landis, C. R. *Organometallics* **2001**, *20*, 2374.

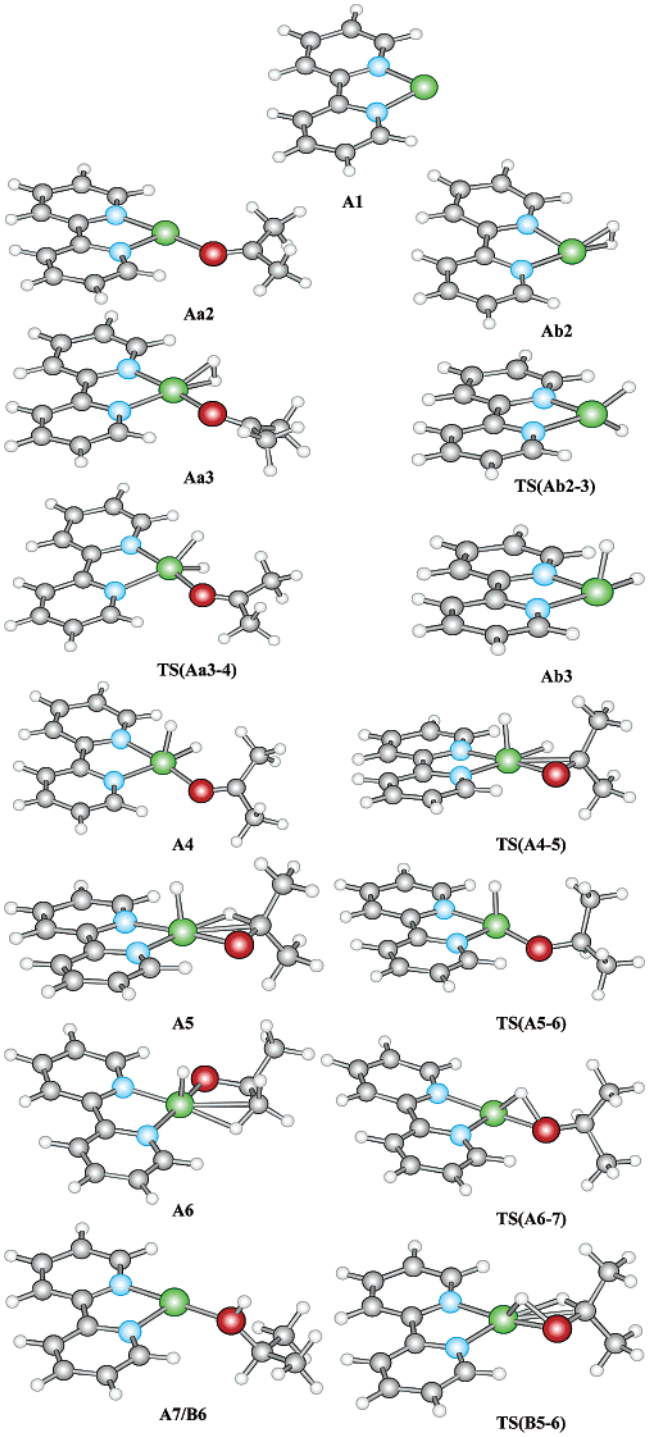

Figure 1. Calculated structures of the intermediates and transition states belonging to Cycles A and B. (Color scheme: green: Rh; gray: C; blue: N; red: O; white: H)

kinetics at the reaction temperature. **TS(A4−5)** has an imaginary frequency of 583i cm^{-1} appropriate for this reaction. The interatomic distances and angles for this step are listed in Table 3.

The second transition state, **TS(A5−6)**, corresponds to the rotation of the alkoxy ligand and has an imaginary frequency of 50i cm^{-1}. The third transition state, **TS(A6−7)**, belongs to the O−H reductive elimination step, which has an imaginary frequency of 997i cm^{-1}. During the formation of the transition state, the agostic interaction of the metal center with the methyl

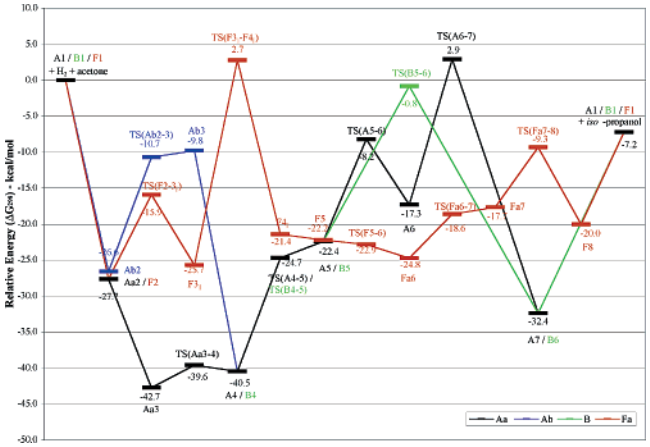

Figure 2. Reaction profiles (ΔG_{298}, in kcal/mol, mPW1K/SDB-cc-pVDZ//mPW1K/SDD) of Cycles A, B, and Fa.

Table 3. Key Interatomic Distances (Å) and Angles (°) Involved in the C−H Coupling in Cycle A

	A4	TS(A4–5)	A5
$Rh-H_{eq}$	1.555	1.648	1.802
Rh−C	3.073	2.337	2.348
$C-H_{eq}$	3.115	1.588	1.258
$C-Rh-H_{eq}$	76.9	42.8	32.0

Table 4. Key Interatomic Distances (Å) and Angles (°) Involved in the O−H Coupling Step of Cycle A

	A6	TS(A6–7)	A7
$Rh-H_{ax}$	1.497	1.561	2.710
Rh−O	1.931	2.007	2.105
$O-H_{ax}$	2.642	1.515	0.965
$O-Rh-H_{ax}$	100.1	48.3	18.1

C−H bond is broken. Table 4 shows the key interatomic distances and angles for the reaction. The final 2-propanol ligand dissociation step is expected to proceed without a barrier.

The loss of 2-propanol is highly endothermic requiring $\Delta G_{298} = 25.2$ kcal/mol. A probable explanation to this high energy is the fact that the product, $[(bpy)Rh]^+$, is a 12 electron complex that would rather have two additional ligands. It is reasonable that this deligation energy can be reduced if one of the incoming ligands for the next cycle were to bind prior to loss of 2-propanol. This is plausible as the reaction is carried out in solution. This leads to four new variants of this catalytic cycle.

As the reaction is carried out in an acetone solution, it is logical that the incoming ligand may be acetone (Cycle Ac). In this case, after the formation of $[(bpy)Rh(^iPrOH)]^+$ (**A7**), acetone ligation yields $[(bpy)Rh(^iPrOH)(ace)]^+$ (**Ac8**) with a reaction energy of $\Delta E = -31.9$ kcal/mol or $\Delta G_{298} = -19.0$ kcal/mol. After the loss of 2-propanol, the catalytic cycle is re-entered at point **Aa2**. Now the loss of 2-propanol requires only $\Delta E = 29.4$ kcal/mol or $\Delta G_{298} = 16.5$ kcal/mol.

In a similar fashion, the incoming ligand can be hydrogen. In Cycle Ad, the incoming hydrogen forms a $\sigma-H_2$ complex, $[(bpy)Rh(^iPrOH)(\sigma-H_2)]^+$ (**Ad8**), prior to loss of 2-propanol. Here, the complex re-enters the catalytic cycle at **Ab2**. The formation of the $\sigma-H_2$ complex has a reaction energy of $\Delta E = -26.8$ kcal/mol or $\Delta G_{298} = -14.5$ kcal/mol, whereas the loss of 2-propanol from this complex requires $\Delta E = 26.5$ kcal/mol or $\Delta G_{298} = 13.1$ kcal/mol. Likewise, the loss of 2-propanol can follow H−H bond activation and the complex can re-enter the

Table 5. Key Interatomic Distances (Å) and Angles (°) in the O−H Coupling Step of Cycle B

	B5	TS(B5−6)	B6
Rh−H_{ax}	1.493	1.578	2.710
Rh−O	1.965	2.021	2.105
O−H_{ax}	2.626	1.451	0.965
O−Rh−H_{ax}	97.9	45.5	18.1

catalytic cycle at point **Ab3**. This can lead to two complexes, one where the axial hydride is on the same side of the bpy plane (i.e., syn) as the 2-propanol OH (Cycle Ae) or on the opposite side (i.e., anti, Cycle Af). The formation of the dihydride complex **Ae9** involves a $\Delta E = 3.2$ kcal/mol or $\Delta G_{298} = 3.1$ kcal/mol, whereas for **Af9**, $\Delta E = 3.5$ kcal/mol or $\Delta G_{298} = 3.7$ kcal/mol. In both cases the reaction barriers are very low and cannot be precisely determined at the mPW1K/SDB-cc-pVDZ//mPW1K/SDD level, but at the mPW1K/SDD level, they are $\Delta E^{\ddagger} = 3.0$ kcal/mol. The loss of 2-propanol from the dihydride complexes requires $\Delta E = 23.3$ kcal/mol or $\Delta G_{298} = 10.0$ kcal/mol from **Ae9**, or $\Delta E = 23.7$ kcal/mol or $\Delta G_{298} = 9.4$ kcal/mol from **Af9**.

In each of the four new variants Ac−f, the energy required for loss of 2-propanol is dramatically reduced. One cannot determine which of the four variants Ac−f actually prevails—a largely academic question in view of the small differences involved—but it is reasonable to assume that all actually transpire in practice. **TS(A6−7)**, the transfer of H_{ax} to the oxygen, may appear to be the rate determining step with $\Delta G^{\ddagger}_{298} = 20.2$ kcal/mol. As **A5**, however, represents a very shallow minimum on the potential energy surface, one has to consider the entire uphill climb from **A4** to **TS(A5−6)** as a pseudo-single step of $\Delta E^{\ddagger} = 28.0$ kcal/mol or $\Delta G^{\ddagger}_{298} = 32.3$ kcal/mol.

In Cycle A, a rotation of the alkoxy ligand, **TS(A5−6)**, takes place between the first and second C−H reductive eliminations. In Cycle B, the second coupling step, transfer of H_{ax} to the oxygen, follows directly from the initial transfer *without this rotation*. This cycle, which is depicted in Scheme 2, starts out the same as Cycle A and only diverges from it at point **TS(B5−6)**, the direct transfer of H_{ax} to the oxygen. In the transition state, H_{ax} is bent toward the oxygen, and the reaction coordinate frequency 1267i cm^{-1} is appropriate for the reaction. The product of the reaction, **B6**, is the same 2-propanol complex as in Cycle A (i.e., **A7**). Table 5 lists the key geometric data for this part of the reaction. **TS(B5−6)** is depicted in Figure 1.

As with Cycle A, here one can propose the same set of variants that only differ in the order that ligands associate or dissociate. Akin to Cycle A, the intermediate **B5** is a shallow minimum on the potential energy surface. Therefore, one has to consider the barrier between **B4** and **TS(B5−6)** as a pseudo-single step of $\Delta E^{\ddagger} = 38.0$ kcal/mol or $\Delta G^{\ddagger}_{298} = 39.6$ kcal/mol. Cycle B has a higher barrier than Cycle A, yet the latter has a subsequent barrier (**A6-TS(A6−7)**, $\Delta G^{\ddagger}_{298} = 20.2$ kcal/mol) that is higher than for the reverse reaction **A6-TS(A5−6)** ($\Delta G^{\ddagger}_{298} = 9.1$ kcal/mol). Thus, Cycle B will in fact be preferred over Cycle A (analogous to refs 43−45), as can easily be verified by solving the system of classical coupled first-order kinetic equations involving **A5**⇌**A6**⇌**A7** and **B5**(=**A5**)⇌**B6**(=**A7**). With the parameters given here, we find that the time dependence of the concentration of A7/B6 is pseudo-first order with a reaction rate that corresponds to an effective Eyring activation energy of $\Delta G^{\ddagger}_{298} = 21.6$ kcal/mol, which is equal to the barrier above for **B5-TS(B5−6)**.

Scheme 3. Reaction Pathway for Cycles D and E[a]

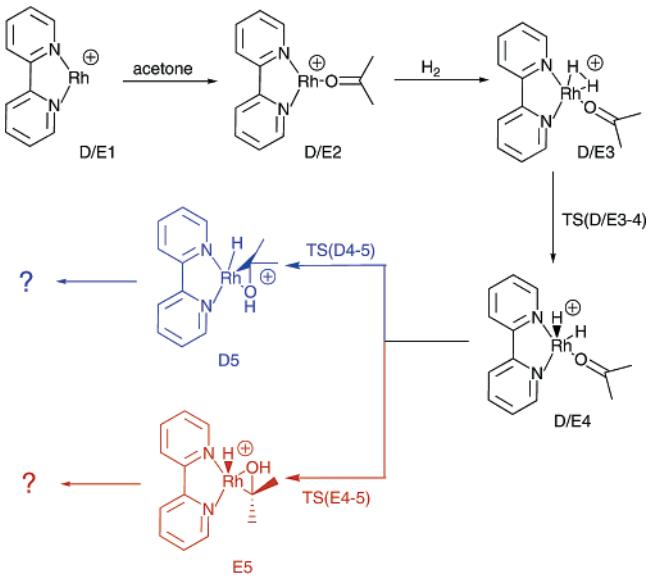

[a] Complexes in blue belong to Cycle D and in red to Cycle E, whereas complexes common to both are in black.

Catalytic Cycle C: Initial Transfer of H_{ax} to the Carbonyl Carbon of Acetone. The initial transfer of H_{ax} to the carbonyl carbon would be the logical complement to Cycles A and B where the initial transfer involved H_{eq}. Nevertheless, despite several attempts at such a reaction pathway, our attempts to find intermediates for this cycle failed. This may be a direct result of the geometry of [(bpy)Rh(ace)H_2]$^{+}$ where such a transfer would bring the hydrogen very close to the acetone oxygen.

Catalytic Cycles D and E: Initial Transfer to the Carbonyl Oxygen of Acetone. Two additional cycles involving the acetone tautomer were also considered. They are depicted in Scheme 3. These two cycles start off the same as Cycle A and diverge at the respective intermediates **D4** and **E4**, specifically [(bpy)Rh(ace)H_2]$^{+}$.

In Cycle D, H_{ax} is transferred to the carbonyl oxygen giving the 2-hydroxy-2-propyl complex **D5**. The reaction energy for this step is $\Delta E = 13.0$ kcal/mol or $\Delta G_{298} = 17.6$ kcal/mol. This step has a transition state, **TS(D4−5)**, that results in a barrier of $\Delta E^{\ddagger} = 36.6$ kcal/mol or $\Delta G^{\ddagger}_{298} = 37.4$ kcal/mol. The transition state has an imaginary frequency of 1514i cm^{-1}. Table 6 lists the key geometric data for this step. Because of the large barrier height obtained, this reaction pathway was not further investigated.

In the initial step of Cycle E, H_{eq} is transferred to the carbonyl oxygen. The key geometric data are listed in Table 7. The reaction energy here is $\Delta E = 12.7$ kcal/mol or $\Delta G_{298} = 16.4$ kcal/mol. The transition state has an imaginary frequency of 1235i cm^{-1}. The barrier height for this step is $\Delta E^{\ddagger} = 51.6$ kcal/mol or $\Delta G^{\ddagger}_{298} = 51.2$ kcal/mol, and therefore, this cycle was not considered further.

Catalytic Cycle F: The Enolic Routes. The reduction of acetone to 2-propanol can be viewed as either: (a) hydrogenation of the C=O bond of acetone, or (b) hydrogenation of the C=C bond of its enol tautomer. Here, we consider the second option.

Scheme 4. Keto−Enol Isomerization Step of Cycle F

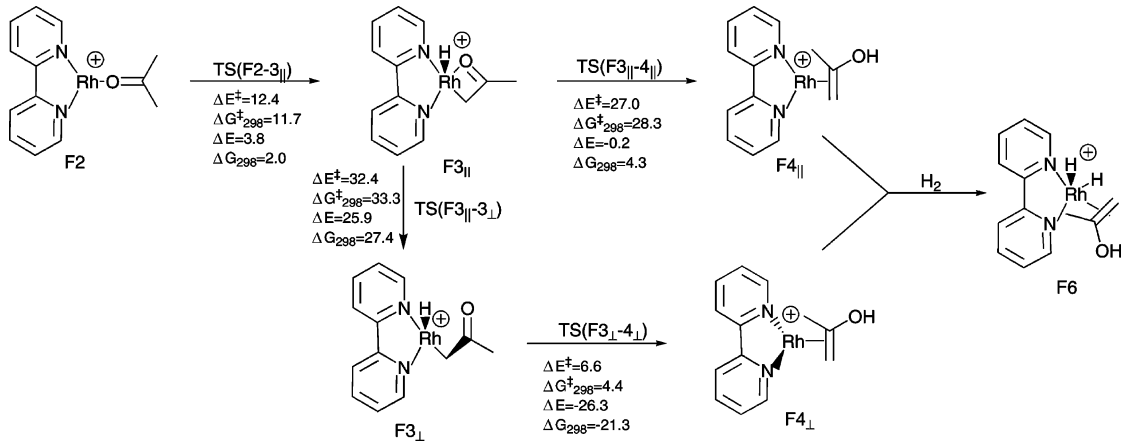

Table 6. Key Interatomic Distances (Å) and Angles (°) Involved in the O−H Coupling Step of Cycle D

	D4	TS(D4–5)	D5
Rh−H_{ax}	1.499	1.836	2.715
Rh−O	2.045	2.111	2.118
O−H_{ax}	2.658	1.298	0.970
Rh−C(internal)	3.073	2.107	1.990
O−Rh−H_{ax}	96.0	37.6	18.3
O−Rh−C(internal)	16.4	38.3	41.8

Table 7. Key Interatomic Distances (Å) and Angles (°) Involved in the O−H Coupling Step of Cycle E

	E4	TS(E4–5)	E5
Rh−H_{eq}	1.555	1.625	2.737
Rh−O	2.045	2.143	2.085
O−H_{eq}	2.598	1.362	0.968
O−Rh−H_{eq}	91.4	39.4	17.2

The solution concentration of the enol tautomer is very low, and therefore the mechanism for the rhodium-catalyzed tautomerization was investigated. Scheme 4 shows the mechanism obtained and the calculated energetics. Two isomers of the enol complex (**F4**) were found, one where the enol C═C bond is angled with respect to the bpy plane (**F4**$_{||}$) and the second where it is perpendicular (**F4**$_{\perp}$). This is one of the points from which sprout the different catalytic cycle variants.

The route to both **F4** isomers start out the same. The initial step is the formation, from $[(bpy)Rh]^+$ (**F1**), of the ligated complex, $[(bpy)Rh(ace)]^+$ (**F2**). The initial oxygen-bound acetone complex (**F2**) undergoes activation of one of the methyl C−H bonds leading to an alkyl hydride complex (**F3**$_{||}$). In this complex, the alkyl ligand is coplanar with the bpy plane. The transition state for this step, **TS(F2−3**$_{||}$**)**, is similar to the product with the hydride already on the metal center and bent toward the carbon whence it came. The transition state has an imaginary frequency of 856i cm^{-1} corresponding to the expected reaction.

O−H reductive elimination from **F3**$_{||}$ will lead to **F4**$_{||}$. The product has the enol C═C bond at an approximate angle of 45° to the bpy plane and an interaction between the Rh and the oxygen. The transition state, **TS(F3**$_{||}$**−4**$_{||}$**)**, for this step involves the transfer of the hydride, which resides in the axial position, to the oxygen.

Alternatively, **F3**$_{||}$ can undergo rotation of the alkyl ligand to give the perpendicular isomer **F3**$_{\perp}$. This alkyl complex, in contrast to **F3**$_{||}$, is not stabilized by the Rh−O interaction, and this probably accounts for the endothermicity and the high barrier for the reaction. From here, reductive O−H elimination leads to the perpendicular isomer **F4**$_{\perp}$. **F4**$_{||}$ is the more stable isomer by $\Delta E = -6.4$ kcal/mol or $\Delta G_{298} = -6.2$ kcal/mol.

Table 8. Various Variants of Cycle F

		orientation with respect to the enol O		
variant	enol orientation	H_{ax}	H_{eq}	initial H transfer
a	parallel	anti	syn	H_{eq} → Internal C
b	parallel	syn	syn	H_{eq} → Internal C
c	parallel	anti	anti	H_{eq} → Terminal C
d	parallel	syn	anti	H_{eq} → Terminal C
e	perpendicular	syn	syn	H_{ax} → Internal C
f	perpendicular	syn	anti	H_{ax} → Internal C
g	perpendicular	anti	anti	H_{ax} → Terminal C
h	perpendicular	anti	syn	H_{ax} → Terminal C

The next step in this cycle is the addition of hydrogen to the enol complex **F4**. As with previous cycles, the dihydride complex **F6** is formed via the σ-H_2 complex **F5** and the transition state for H−H bond activation, **TS(F5−6)**. **F6** has several isomeric structures and this leads to several catalytic cycle variants because both the axial and the equatorial hydrides may each be either syn or anti (vide supra) with respect to the enol oxygen. Furthermore, in **F6** the enol ligand may be either parallel or perpendicular to the bpy plane. Here, in the case of the parallel mode, the enol is much more planar than before, such that we feel justified in using the term parallel rather than angled. There are two other sources that generate additional variants. There are two hydride ligands, H_{ax} and H_{eq}, either of which may be involved in the initial hydrogen transfer step. Likewise, the initial transfer may be either to the internal or to the terminal carbon of the enol double bond. All these permutations lead to a plethora of variants, in theory $2^5 = 32$. Many of these permutations were examined and these are listed in Table 8. Some of the others were not examined because they would involve geometrically unreasonable steps, such as a hydride passing through chemical bonds. Moreover, it became readily apparent that the common rate determining step of all the different variants takes place during the keto−enol tautomerization (vide infra).

From **F6**, the two hydrogen transfers yield the intermediate hydroxyalkyl complex (**F7**) and the 2-propanol complex (F8), respectively. The transition states for each transfer were identified and verified by IRC calculations and lead to barriers

Table 9. Reaction Data for the Various C−H Coupling Steps in Cycle F[a]

	1st C–H coupling step			2nd C–H coupling step		
variant	ΔG_{298}	$\Delta G^{\ddagger}_{298}$	frequency	ΔG_{298}	$\Delta G^{\ddagger}_{298}$	frequency
a	7.1	6.1	391i	−2.4	8.4	725i
b	6.1	4.6	382i	−3.1	8.7	707i
c	0.3	3.0	537i	−0.9	6.8	669i
d	1.3	4.7	572i	−1.6	8.3	598i
e	11.4	16.1	376i	−10.0	2.1	706i
f	9.1	13.7	635i	−6.2	4.0	775i
g	2.2	9.9	825i	2.2	9.4	585i
h	1.4	8.4	793i	0.4	10.6	609i

[a] Energies are in kcal/mol and frequencies in cm^{-1}.

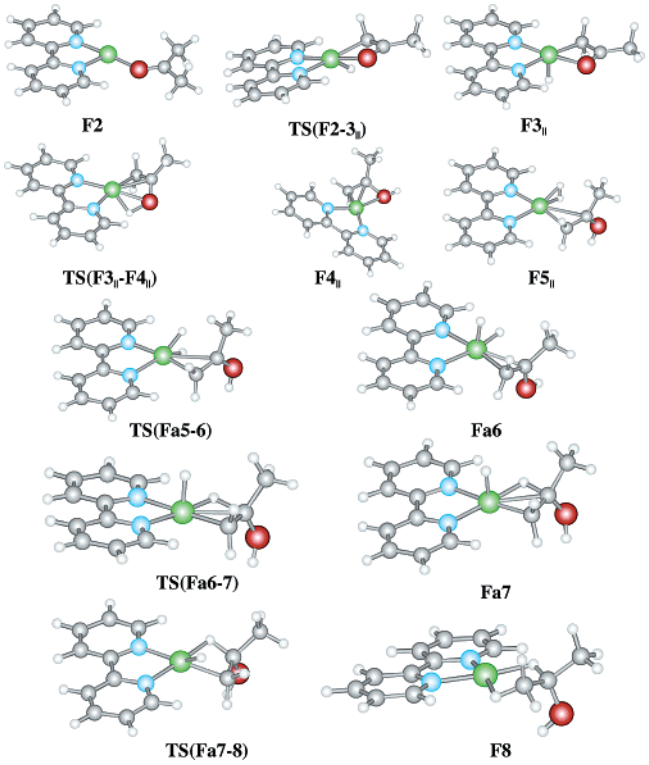

Figure 3. Calculated structures of the intermediates and transition states for Cycle Fa. See Figure 1 for color scheme.

of $\Delta G^{\ddagger}_{298} = 4 \sim 17$ kcal/mol. Table 9 lists the reaction energies, reaction barriers and the transition state imaginary frequencies of each C−H coupling step of each enolic variant studied. As an example, Figure 3 depicts the geometries of the complexes belonging to Cycle Fa. In contrast to the analogous complex **A7** or **B6** where the 2-propanol is bound through the oxygen, this complex (**F8**) has the ligand bound through two agostic C−H interactions involving the two newly formed C−H bonds. This binding mode is higher in energy than **A7** or **B6** as evident from the ligand dissociation energy of $\Delta E = 25.3$ kcal/mol or $\Delta G_{298} = 12.8$ kcal/mol.

In each case, the rate determining step for the reaction in Cycle F is part of the keto−enol tautomerization step. For the cases of the parallel enol, it is the transfer of the hydrogen to the oxygen, **TS(F3∥−F4∥)**. For the cases of the perpendicular enol, it is the alkyl rotation from the planar to perpendicular mode, **TS(F3∥−3⊥)**. This leads to barriers of $\Delta G^{\ddagger}_{298} = 28.3$ kcal/mol or $\Delta G^{\ddagger}_{298} = 33.3$ kcal/mol, respectively. Even if one were to consider the intermediates **F5**, **F6**, and **F7** as shallow minima, the aggregate barrier thus obtained would still be smaller than 20 kcal/mol. In this case, in contrast to Cycles A and B, there is no issue of a subsequent barrier comparable to or higher than the reverse reaction that would force the reaction to proceed back to the starting materials. It is apparent that the preferred variants of Cycle F involve the enol ligand adopting a parallel orientation, that is Cycles Fa−d. As the differences between the variants occur after the rate determining step, and are anyhow small, the question of which variant actually occurs is mostly academic. As an example, the reaction profile of variant Fa is depicted in Figure 2.

Table 10. Reaction Profile (kcal/mol) for the Keto−Enol Tautomerisation of Cycle I

transition	description	ΔG_{298}	$\Delta G^{\ddagger}_{298}$
I1−I2	acetone ligation	−21.0	[a]
I2−I3	C−H activation	12.8	28.5
I3−I4	O−H coupling	−2.1	32.9

[a] No transition state.

Inclusion of a Solvent Molecule in the Reaction Profile: Cycles G, H, and I. Although solvation effects are difficult to model, one effect can be easily accounted for. It is quite reasonable that the solvent can coordinate to the various complexes, and in fact, all of the complexes have a site available for solvent coordination and many would be stabilized by this. Two solvent molecules are of special interest here: water and acetone. The former is of interest as the multi-center (monolayer) reaction takes place in an aqueous acetone solution, whereas the latter is of interest because the uni-center reaction is carried out in acetone.

The keto−enol isomerization that comprises the first part of Cycle F was examined with the addition of a water solvent molecule. This leads to Cycle I and only the more stable parallel enol isomer (vide supra) was considered. The results with acetone can be expected to be similar. Table 10 lists the reaction energies for this part of the cycle. From the results, it can be concluded that this is not a plausible mechanism as the barrier for O−H coupling, **TS(I3−4)**, is too high at $\Delta G^{\ddagger}_{298} = 32.9$ kcal/mol. In addition, the water-rhodium bond lengths in the transition states are considerably lengthened compared to the intermediates. In the transition states, these lengths are 2.564 and 2.584 Å, respectively, whereas in the intermediates, they are 2.118, 2.135, 2.242, and 2.107 Å, respectively. This would indicate that this tautomerization proceeds without solvent coordination, and this is not surprising as the rhodium center is stabilized by an interaction with the enolic oxygen, whereas in the acetone catalytic cycles, there are weaker agostic-type interactions. It is not expected that the inclusion of a spectator solvent ligand in the second half of the catalytic cycle would raise the barriers sufficiently as to make an acetone route viable. This is especially true as the solvent is intended to stabilize the complexes, and thus lower the reaction barriers. If the reaction with a solvent is less favorable, as it would appear to be here, then the reaction can simply proceed without the additional spectator ligand. Therefore, the only question that remains is whether the addition of a solvent molecule can sufficiently improve the acetone-type catalytic cycles so to make them viable.

The two more likely reaction acetone-type catalytic cycles (Ab and B) were thus reexamined with the inclusion of a spectator solvent molecule. The addition of water or acetone to Cycle Ab gives Cycles Ga and Gb, respectively, while from

Table 11. Reaction Energies (ΔG_{298}, kcal/mol) and Barrier Heights ($\Delta G^{\ddagger}_{298}$, kcal/mol) for the Various Steps in Cycles G and H

	Cycle G			Cycle H	
transition	a (H_2O)	b (acetone)	transition	a (H_2O)	b (acetone)
G1−G2	−16.0	−15.1	H1−H2	−16.0	−15.1
G2−TS(G2−3)	1.5	3.1	H2−TS(H2−3)	1.5	3.1
G2−G3	3.6	1.9	H2−H3	3.6	1.9
G3−G4	−13.1	−7.8	H3−H4	−13.1	−7.8
G4−TS(G4−5)	[a]	[a]	H4−TS(H4−5)	[a]	[a]
G4−G5	15.9	16.9	H4−H5	15.9	16.9
G5−TS(G5−6)	[b]	[b]	H5−H5′	−2.5	−7.1
G5−G6	4.5	2.8	H5′−TS(H5′−6)	15.1	16.3
G6−TS(G6−7)	8.4	6.9	H4−TS(H5′−6)[c]	31.0	28.3
G4−TS(G6−7)[d]	31.3	28.7	H5′−H6	−15.4	−15.0
G6−G7	−22.4	−24.9	H6−H1 + ^{i}PrOH	17.7	16.5
G7−G1 + ^{i}PrOH	17.7	16.5			

[a] Barrier too small to be accurately determined; see text. [b] Transition state could not be located; see text. [c] Considering **H5** and **H5′** as shallow minima on the potential energy surface; see text. [d] Considering **G5** and **G6** as shallow minima on the potential energy surface; see text.

Cycle B, Cycles Ha and Hb are likewise obtained. Table 11 lists the reaction energies and barrier heights for the various steps in these cycles. Fundamentally, these steps are very similar to their nonsolvated counterparts. In general, the reactions involving the association or dissociation of ligands have smaller absolute reaction energies. This is expected as the solvated complexes have the additional ligand that helps stabilize the complexes. The H−H bond activation barrier is likewise considerably lower when the extra ligand is added; a similar observation can be made when comparing Cycles Aa and Ab. Overall, the stabilizations afforded by water and by acetone are of a similar level.

One significant difference between the solvated and nonsolvated reaction pathways is the barrier to O−H coupling. In the nonsolvated pathways, this step had a high barrier (∼20 kcal/mol). In the solvated reaction pathways, however, this barrier is considerably lower; this may result from the fact that the product of this step, [(bpy)Rh(^{i}PrOH)L]$^+$ (either **G7** or **H6**, L = ace or H_2O), is a 16 electron, d^8 square planar Rh(I) complex. The stability afforded by such a complex helps lower the associated barrier heights.

Another key difference between Cycles H and B is the presence of an additional intermediate in the former. In the first part of the reaction, the solvent ligand resides in an axial position until intermediate **H5**. This is the intermediate directly prior to O−H coupling and still has the solvent molecule in the axial position even though there is a vacant equatorial position. Migration of the solvent molecule to this position yields the more stable intermediate **H5′**.

As the O−H coupling step is not rate determining, the differences between the reaction profiles of Cycles G and H, for the respective solvents, are not significant. The barrier for the C−H coupling step, **TS(G** or **H4−5)** could not be exactly determined at the mPW1K/SDB-cc-pVDZ//mPW1K/SDD level because the reverse reaction has a small barrier. Likewise, due to the size of the system and its flexibility, the transition state for the rotation of the alkoxy ligand, **TS(G5−6)**, could not be located, although it is expected that this rotation should not have an overly high barrier. However, as with Cycles A and B, the minima corresponding to the C−H coupling products, specifically **G5** and **G6**, and **H5** and **H5′**, have to be considered as shallow minima on their respective potential energy surfaces due to the low reverse reaction barriers. Thus one must consider the rate determining barriers as **G4** to **TS(G6−7)** and **H4** to **TS(H5′−6)**. These barriers thus obtained, as shown in Table 11, are considerably lower than in the respective cases without a spectator solvent ligand, to the point where the acetone route becomes competitive with the enol route, especially in the case where the solvent is acetone. In fact, in this scenario, the barriers are approximately equal to the rate determining barrier in Cycle Fa−d.

Scheme 5. Model Ligand Systems Examined

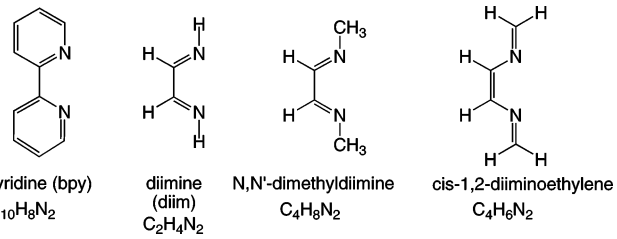

Table 12. Cycle Ab Reaction Energies and Barrier Heights for the Various Ligand Systems[a]

	bpy	diimine	diiminoethylene	dimethyldiimine
A1−A2	−26.6	−15.8	−16.6	−14.2
A2−TS(A2−3)	15.9	6.1	5.7	6.3
A2−A3	16.8	7.7	6.8	7.8
A3−A4	−30.7	−35.9	−33.2	
A4−TS(A4−5)	15.7	20.3	17.7	
A4−A5	18.1	22.6	20.2	
A5−TS(A5−6)	14.2	17.0	14.7	
A5−A6	5.1	6.2	5.3	
A6−TS(A6−7)	20.2	11.8	14.5	
A6−A7	−15.1	−22.8	−17.0	
A7−A1 + ^{i}PrOH	25.2	30.7	27.2	
A4−TS(A5−6)	32.3	39.6	34.9	

[a] All energies are ΔG_{298} or $\Delta G^{\ddagger}_{298}$, as appropriate, in kcal/mol.

Model Systems. Having thoroughly investigated the solution reactivity of [(bpy)Rh]$^+$, the next step in the investigation is the multi-center reaction system. The bpy ligand ($C_{10}H_8N_2$) is far too large to allow for feasible calculations with more than one [(bpy)Rh]$^+$ center. We therefore compared the calculated reactivity of three model ligands against the bpy ligand. The model ligands examined are depicted in Scheme 5.

Two of the cycles were investigated: the most plausible acetone catalytic cycle, Cycle A, and one of the enolic cycles, Cycle Fa. Initially, the comparison focused on the addition of hydrogen to the Rh center in Cycle Ab. At each point along the reaction pathways, including the transition states, the geometries were reoptimized using each new model ligand. From this, it was apparent that the dimethyldiimine ligand, as well as being the largest, did not perform any better than the other two. Next, the entire Cycles Ab and Fa were compared using the other two model ligands. Tables 12 and 13, respectively, list the reaction profiles for each catalytic cycle for the various ligand systems. From the reaction profiles, it is clear that the other two ligands perform satisfactorily. Although the diiminoethylene ligand outperforms the diimine ligand in the comparison with bpy, the latter has the distinct advantage of being significantly (30%) smaller. One can greatly capitalize on this smaller size in calculations involving multi-center systems (vide infra).

Table 13. Cycle Fa Reaction Energies and Barrier Heights for the Various Ligand Systems[a]

	bpy	diimine	diiminoethylene
F1−F2	−27.7	−34.1	−27.7
F2−TS(F2−3$_{II}$)	11.7	16.0	12.6
F2−F3$_{II}$	2.0	8.8	4.2
F3$_{II}$−TS(F3$_{II}$−4$_{II}$)	28.3	27.4	27.8
F3$_{II}$−F4$_{II}$	4.3	−0.5	2.7
F4$_{II}$−F5$_{II}$	−0.8	−7.4	−7.0
F5$_{II}$−TS(Fa5−6)	[b]	5.1	4.5
F5$_{II}$−Fa6	−2.5	3.6	2.1
Fa6−TS(Fa6−7)	6.1	9.1	7.8
Fa6−Fa7	7.1	9.8	8.7
Fa7−TS(Fa7−8)	8.4	8.9	8.9
Fa7−Fa8	−2.4	−3.7	−2.0
Fa8−F1 + ^{i}PrOH	12.8	16.4	14.1

[a] All energies are ΔG_{298} or $\Delta G^{\ddagger}_{298}$, as appropriate, in kcal/mol. [b] Barrier too small to be precisely determined; see text.

Table 14. Comparison of CCSD(T) and mPW1K Calculated Energies[a]

	CCSD(T)/SDB-cc-pVDZ		mPW1K/SDB-cc-pVDZ	
complex	ΔE_e	ΔG_{298}	ΔE_e	ΔG_{298}
A4 / F2	0.0	0.0	0.0	0.0
TS(A4−5)	18.4	20.2	18.4	20.2
A5	19.3	22.3	19.6	22.6
TS(A5−6)	35.5	39.9	35.1	39.6
A6	23.7	28.6	24.0	28.9
TS(A6−7)	36.7	40.4	37.0	40.7
A7	7.1	11.8	1.4	6.1
A4−TS(A5−6)	35.5	39.9	35.1	39.6
TS(F2−3$_{II}$)	11.8	11.8	16.1	16.0
F3$_{II}$	3.4	3.8	8.5	8.8
TS(F3$_{II}$-F4$_{II}$)	30.6	30.5	36.3	36.2
F4$_{II}$	3.6	7.1	4.8	8.3
F3$_{II}$−TS(F3$_{II}$−F4$_{II}$)	27.2	26.8	27.8	27.4

[a] All calculations use the SDB-cc-pVDZ basis set and the mPW1K/SDD reference geometries with the diimine model ligand. All energies are in kcal/mol and relative to **A4** or **F2** as appropriate.

Calibration Calculations and Inclusion of Bulk Solvent Effects. To better assess the accuracy of the calculations, CCSD(T)/SDB-cc-pVDZ single point energy calculations were carried out on the mPW1K/SDD reference geometries of the hydrogen transfer steps of Cycle A (i.e., **A4**-**A7**) and the keto−enol tautomerization step of Cycle F (i.e., **F2**-**F4**$_{II}$). However, as CCSD(T) calculations scale very steeply with the size of the system, using the full bpy ligand would be far beyond our computational ability. It was therefore necessary to utilize the diimine model ligand in the CCSD(T) calculations. Table 14 lists the CCSD(T) energies relative to **A4** or **F2** as appropriate. These data are compared to the relevant mPW1K data and one can clearly observe that overall there is excellent agreement between the two methods. As CCSD(T) is considered to provide accurate energies, one can thus rely on the mPW1K data to be accurate.

So far, all of the calculations are in the gas phase. It is common practice to investigate solution reactions in the gas phase and assume that the reaction in solution follows a similar pathway. Although it would be ideal to include solvent effects in the calculations, the methods available involve significantly higher computational cost and many crude approximations. Nevertheless, single point energy calculations using the mPW1K/SDD reference geometries were done using two solvation models, specifically PCM and COSMO (see Computational Details section) using acetone as the solvent.

Table 15. Calculation of Key of Cycles A, B, F, Gb, and Hb Using the PCM and COSMO Solvation Models at the mPW1K/SDB-cc-pVDZ//MPW1K/SDD Level of Theory[a]

	PCM		COSMO	
complex	ΔE_e	ΔG_{298}	ΔE_e	ΔG_{298}
A4 / B4 / F2	0.0	0.0	0.0	0.0
TS(A4−5)	13.7	14.9	13.2	14.4
A5/B5	13.6	16.4	12.4	15.3
TS(A5−6)	23.1	27.3	21.6	25.8
TS(B5−6)	35.7	37.3		
A6	15.6	20.1	15.0	19.5
TS(A6−7)	37.4	38.8	36.1	37.5
A7 / B6	1.1	5.2	−0.1	4.1
A4−TS(A5−6)	23.1	27.3	21.6	25.8
B4−TS(B5−6)	35.7	37.3		
TS(F2−3$_{II}$)	11.6	10.9	12.2	11.5
F3$_{II}$	4.2	2.4	4.3	2.5
TS(F3$_{II}$-F4$_{II}$)	30.0	29.5	30.6	30.1
F4$_{II}$	1.2	3.9	2.0	4.7
F3$_{II}$–TS(F3$_{II}$-F4$_{II}$)	25.7	27.0	26.3	27.6
TS(GorHb4−5)	17.8	18.6		
Gb5 / Hb5	19.0	21.0		
Gb6	18.4	22.9		
TS(Gb6−7)	27.8	29.7		
Hb5′	8.9	13.2		
TS(Hb5′-6)	27.4	29.5		
Gb7 / Hb6	−5.6	−1.9		
Gb4−TS(Gb6−7)	27.8	29.7		
Hb4−TS(Hb5′−6)	27.4	29.5		

[a] All energies are in kcal/mol and relative to **A4** or **F2** as appropriate.

Key parts of Cycles A, B, Fa, Gb, and Hb were recalculated using the PCM method. These results are summarized in Table 15. In addition, the COSMO method was used to recalculate Cycles A and Fa in order to gauge the sensitivity of the calculated solvent effects on the solvation treatment used. Overall, the agreement between the two methods is outstanding. The effect of solvation on Cycles Fa, Gb, and Hb is small, less than 1.5 kcal/mol. If one were again to solve, for Cycles A and B, the system of classical coupled first-order kinetic equations (vide supra), one would obtain an effective barrier of $\Delta G^{\ddagger}_{298} = 37.3$ kcal/mol (PCM model). Therefore, these two cycles are still not competitive with Cycles Fa, Gb, and Hb that have rate determining barriers of $\Delta G^{\ddagger}_{298} = 27.0$, 29.7, and 29.5 kcal/mol, respectively. Based on the calculations using these solvation models, the three catalytic cycles would appear to be competitive. One must, however, use these results with caution as several approximations have been used, including those intrinsic to the models[33−35,37,46] as well as the use of the gas-phase mPW1K/SDD optimized geometries and G_{298} corrections.

Cooperativity Effects. A reasonable explanation for the reaction rate acceleration in the monolayer system is cooperation between two metal centers. If one were to reexamine Cycle F, a reaction mechanism involving two metal centers would suggest itself. This catalytic cycle (Cycle J) was examined using the diimine (herein diim) model ligand. There are two major clues in Cycle F that lead to Cycle J. The first clue is the two coordination modes of 2-propanol: η^{1-O} (**A7**/**B6**) and $\eta^{4-CH,CH}$ (**F8**). Although, so far, acetone has only adopted the former, there is no reason it cannot adopt the latter as well. A complex where acetone bridges two rhodium centers was found, [(diim)Rh(μ-η^{1-O}:$\eta^{4-CH,CH}$-acetone)Rh(diim)]$^{2+}$ (**J2**) where the acetone simultaneously adopts both coordination modes. The other clue is the perpendicular keto−enol tautomerization

(46) Barone, V.; Cossi, M. *J. Phys. Chem. A* **1998**, *102*, 1995.

Scheme 6. Cooperativity in the Keto−Enol Tautomerisation Catalyzed by $[(diim)Rh]_2^{2+}$ (Cycle J). Energies Are in Kcal/Mol

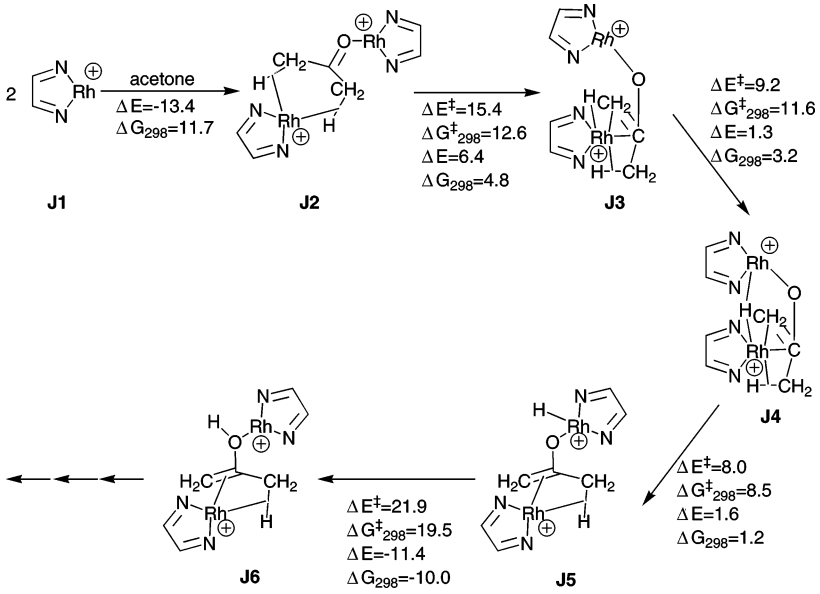

intermediate $\mathbf{F3}_{\perp}$. Its formation is highly endothermic, probably due to the loss of the Rh−O interaction. Nevertheless, the subsequent O−H coupling has a lower reaction barrier from the perpendicular isomer than from the parallel isomer (see Scheme 4). This oxygen, moreover, is perfectly orientated to bridge between two rhodium centers, and if this were to occur, this would eliminate the energetically unfavorable loss of the Rh−O interaction.

The keto−enol tautomerization part of Cycle J was calculated for the bimetallic system. In the experimental system, the long alkyl chains hold the $[(bpy)Rh]^+$ centers in a flexible array (i.e., monolayer). It was also determined that the average spacing between adjacent centers is 4.6 Å and that the degree of order in the monolayer is low.[1] This allows for some flexibility in the system. Unfortunately, we could not enforce these geometrical constraints and the $[(diim)Rh]^+$ centers were allowed to freely orientate themselves in space. Nonetheless, it is not expected that the changes caused by not constraining the centers will be significant. The reorientation to a monolayerlike arrangement would only require facile rotations around single bonds.

Scheme 6 depicts the bimetallic keto−enol tautomerization mechanism found, whereas the various complexes are shown in Figure 4. The first step is the formation of the acetone adduct **J2**. Its formation is not expected to be problematic; initial formation of an η^{1-O}-acetone adduct should position the acetone in close proximity to the second rhodium center allowing easy $\eta^{4-CH,CH}$-coordination to the second metal center. The reaction, from acetone and two individual $[(diim)Rh]^+$ (**J1**) centers is exoenergetic, as expected, by $\Delta E = -13.4$ kcal/mol. On the G_{298} surface, however, one obtains $\Delta G_{298} = +11.7$ kcal/mol. It is not realistic that the formation of **J2** is endothermic and one must remember that this value also includes the entropy loss in forming the monolayer.

The next step is the C−H activation of one methyl C−H bond yielding **J3**. This process is already started by the formation of the agostic bond. Reorientation of the second $[(diim)Rh]^+$ center results in a complex (**J4**) where the hydride ligand bridging between the two rhodium centers, which have become nearly parallel. In the next step, the hydride is transferred to the second rhodium center to give **J5** prior to O−H coupling to give $[(diim)Rh(\mu\text{-}\eta^{1-O}\text{:}\eta^{4-C=C,CH}\text{-enol})Rh(diim)]^{2+}$ (**J6**). From this complex, the reaction proceeds easily to 2-propanol in the monomeric (i.e., Cycle F) system. In Cycle F, the barriers in the hydrogen transfer steps, even if one were to consider the intermediates as shallow minima, never rise above 20 kcal/mol. Therefore, this second part of the reaction does not require assistance from cooperativity effects to be efficient.

In the keto−enol tautomerization part of Cycle J, there are four transition states. These give rise to reaction barriers of

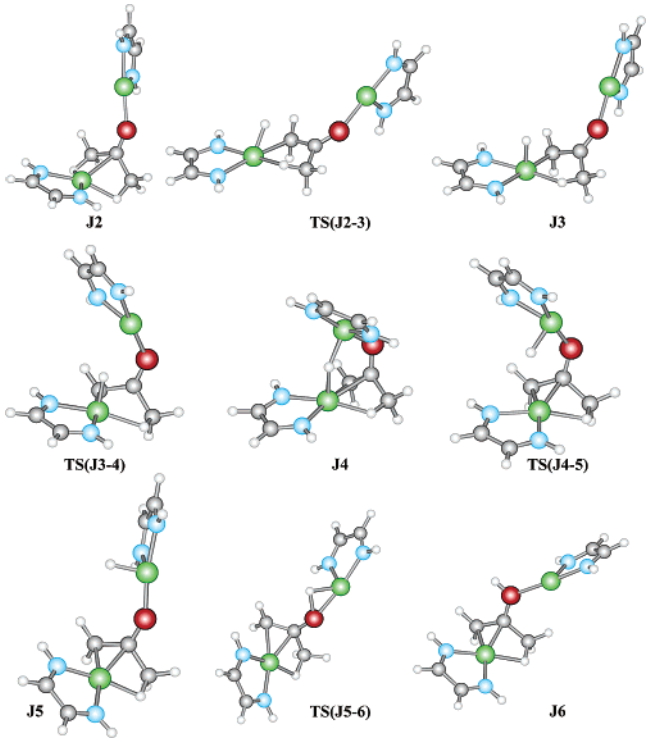

Figure 4. Computed structures of the intermediates and transition states of the keto−enol tautomerization step of the cooperative Cycle J. See Figure 1 for color scheme definition.

$\Delta G^{\ddagger}_{298}$ = 12.6, 11.6, 8.5, and 19.5 kcal/mol. Therefore, the rate determining barrier is $\Delta G^{\ddagger}_{298}$ = 19.5 kcal/mol, considerably lower than in the monomeric system. This substantial lowering of the rate determining barrier, approximately 9 kcal/mol, would, in turn, lead to a substantial enhancement of the reaction rate for the hydrogenation of acetone. As a rough estimate, at room temperature a difference of 1 kcal/mol corresponds to 1 order of magnitude on the rate of reaction. Although the reaction rate of the monomeric system is only 100 times that of the catalyst in solution, the latter takes place in neat acetone while the former is carried out in a 0.11 mM aqueous acetone solution.

If one were to consider any of the acetone routes as a candidate for a cooperativity mechanism, one would quickly see that such a mechanism would not be beneficial. It is readily apparent, especially from the structures of **J2**, **J3**, and **J4** that the acetone carbon is remote and shielded from both rhodium centers by the rest of the acetone molecule. Therefore, hydrogen transfer to this site would be very difficult, and therefore, high in energy.

One problem with this model system is that it cannot quantitatively explain the difference in reactivity in the monolayer system between acetone and butanone. Usually, the addition of a methyl group does not have as dramatic an effect on the reactivity. Qualitatively, it is likely that this difference arises due to steric interactions between the methyl group and the bpy rings. This would be exacerbated by the enol route were both terminal carbons of acetone are held close to the rhodium center. The model system, however, is too flexible and uses the truncated diim ligand, and thus the steric interaction between the methyl group and the bpy ring cannot be calculated.

Conclusions

We reported here on the reaction mechanism of the Rh(I) catalyzed hydrogenation of acetone to 2-propanol as investigated by DFT methods at the mPW1K/SDB-cc-pVDZ//mPW1K/SDD level. Three potential catalytic cycles were identified, specifically Cycles Fa−d, G, and H. The first involves the enol tautomer of acetone. This tautomerization, catalyzed by the [(bpy)Rh]$^+$ complex, was found to have barriers of $\Delta G^{\ddagger}_{298}$ = 11.7 and 28.3 kcal/mol, the second being the rate determining step of the overall catalytic cycle. From here, addition of hydrogen and two C−H coupling steps lead to the final 2-propanol product. Several different pathways for these last steps were examined and all had reaction barriers of less than 20 kcal/mol. The latter two catalytic cycles involve the acetone tautomer and a spectator solvent (acetone) ligand. In these cycles, after formation of the [(bpy)Rh(ace)$_2$(H)$_2$]$^+$ intermediate, initial transfer of H_{eq} to the carbonyl C═O bond yields the 2-propanol product. These catalytic cycles have rate determining barriers of $\Delta G^{\ddagger}_{298}$ = 28.3 (Cycles Fa−d and H) and 28.7 kcal/mol (Cycle G). The accuracy of the mPW1K calculations was confirmed by CCSD(T) calculations on the diimine model system. Other catalytic cycles were considered but they have substantially higher barriers for the rate determining steps.

Bulk solvent effects were considered using the PCM and COSMO solvation models. Both methods yielded similar results. The rate determining sections of Cycles A, B, Fa, Gb, and Hb were reexamined using the PCM model and the results indicate that the latter three catalytic cycles are still competitive.

In addition, three model ligands for the bipyridine (bpy) ligand were considered. *cis*-1,2-diiminoethylene was found to have the best performance of the model ligands examined while the considerably smaller diimine still yields satisfactory results.

Finally, it was shown that the enhanced reactivity of the monolayer system may be explained by cooperation between two rhodium centers. This system was modeled (Cycle J) by [(diim)Rh]$_2^{2+}$, and it was found that the keto−enol tautomerization can be significantly aided by the two centers working in tandem to transfer the hydrogen from the methyl group to the oxygen. It was found that the rate determining step in such a system would be $\Delta G^{\ddagger}_{298}$ = 19.5 kcal/mol, considerably lower than without cooperation between two rhodium centers. In contrast, hydrogen transfer to the carbonyl carbon, in analogue to Cycle A or B, is much more difficult in the dimeric system as this carbon is shielded and remote from either rhodium center. The geometry of this system may also, qualitatively, explain the difference in reactivity between acetone and butanone. In butanone, the extra methyl would likely be in steric conflict with the bpy rings.

Acknowledgment. Research was supported by the Helen and Martin Kimmel Center for Molecular Design, the Minerva Foundation, Munich, Germany, and the *Tashtiyot* (Infrastructures) program of the Ministry of Science and Technology (Israel) as well as by a computer time grant from the (Israel) Inter-University Computer Center. J.M.L.M. is a member of the Lise Meitner-Minerva Center for Computational Quantum Chemistry. M.A.I. acknowledges a Doctoral Fellowship from the Feinberg Graduate School (Weizmann Institute of Science). A.S. was supported by a postdoctoral fellowship from the Minerva Foundation.

Supporting Information Available: Calculated structures, in Xmol (.xyz) format of all complexes, as a text file. This material is available free of charge via the Internet at http://pubs.acs.org or at http://theochem.weizmann.ac.il/web/papers/acetone.html.

JA028489E